Interval methods for lack-of-knowledge uncertainty in crash analysis

Conradus van Mierlo[a,*], Lukas Burmberger[c], Marco Daub[c], Fabian Duddeck[c], Matthias G.R. Faes[a,b], David Moens[a]

[a] *KU Leuven, Department of Mechanical Engineering, Jan De Nayerlaan 5 2860, Sint-Katelijne-Waver, Belgium*
[b] *Institute for Risk and Reliability, Leibniz Universität Hannover, Callinstr. 34, 30167 Hannover, Germany*
[c] *Technical University of Munich, Department of Civil, Geo and Environmental Engineering Arcisstr. 21, 80333 München, Germany*

Abstract

This paper deals with lack-of-knowledge uncertainty in complex non-linear simulations on a component level, i.e., a crashbox during frontal impact of a vehicle. Specifically, the focus lies on using interval field techniques to model the uncertain boundary conditions during impact simulations. The uncertainty considered in this work is the unknown mechanical response from the adjacent structure. This uncertainty is considered to be epistemic, representing the case where this adjacent structure is unknown at the time the impact analysis is performed. In practice, this refers to the situation where the adjacent structure is still under development, e.g., at a different department or even outsourced. In addition, the safety critical performance of both, the component and the overall structure should be guaranteed under a wide range of circumstances, which are typically encountered in real-life situations. Typically, car manufacturers use multidisciplinary optimisation to identify component designs that perform best on all requirements in a deterministic sense, while minimising the overall weight. Unfortunately, the results of such optimisation schemes are known to converge to an often non-robust optimum. As a result, the response of the structure may be sensitive to small changes in input parameters or boundary conditions.

As an answer to these challenges, this paper proposes an interval field approach that accounts for the epistemic, i.e., lack-of-knowledge, uncertainty of the adjacent structures, even in an early design stage. This is accomplished by introducing a spatially varying uncertain mechanical compliance in elements that connect the component to the adjacent structures. These elements have an interval valued stiffness, which is varied along the component following the realisations of an interval field. The bounds on the interval-valued response quantities of interest, i.e., mean force and peak force, are identified using a differential evolution algorithm. This method is demonstrated on four case studies of a full overlap crash analysis of a rectangular crash box, which represents a generic component within the front structure of a vehicle. These case studies demonstrate the applicability and the potential of the proposed method. In addition, in the last case it is shown that the performance of the component can be assessed under an increasing range of uncertainty.

Keywords:
Uncertainty Quantification, interval field, epistemic uncertainty, crashworthiness, lack-of-knowledge uncertainty, impact performance

*Corresponding author
Email address: `koen.vanmierlo[at]kuleuven.be` (Conradus van Mierlo)

1. Introduction

In recent years car manufacturers are changing from traditional test-based design towards more simulation-driven approach due to the ever rising complexity in development and increase of safety requirements. Examples of such safety requirements are, e.g., proposed by the United Nations Economic Commission for Europe (UN-ECE) [1], or based on consumer tests, e.g., those of the New Car Assessment Programmes (NCAP) like Euro NCAP [2] or Global NCAP [3]. These tests represent the relevant accident scenarios while being also sufficiently repeatable to enable controlled vehicle assessments and ratings. In these numerical approaches advanced numerical methods for multi-disciplinary and multi-criteria optimisation are used to identify the appropriate design compromises, see, e.g., [4]. However, even in standard cases, the performance of designs obtained though optimisation are known to be very sensitive to small changes in input parameters. This problem is further amplified when considering highly non-linear phenomena encountered in crashworthiness studies [5]. Furthermore, the robustness - low sensitivity of responses to input variations - as well as the reliability - low probability of constraint violations - have to be considered additionally. This leads to an even higher numerical effort than just needed for a deterministic optimisation.

In addition design criteria for crashworthiness are mostly related to bio-mechanical measures (accelerations, velocities, deformations, forces, and moments) registered by Anthropometric Test Devices (ATDs), also known as “dummies”. Examples are the Head Injury Criterion (HIC), see the discussion in [6], or the Neck Injury Criterion (NIC), see [7]. The optimal quantity to use in crashworthiness assessment is changing frequently, see e.g. [8]. However, during the early development process, it is standard to consider mainly structural criteria, i.e., criteria related to the performance of the car structures, as detailed geometrical and material data is not available. Car-body related criteria address either aspects of the safety cage (deformation resistance parts) or aspects of the crumple zones (energy absorbing parts), as illustrated in Figure 1. The design of energy absorbing parts remains challenging, criteria as specific energy absorption (SEA), which is the total energy absorption divided by mass, peak force or peak acceleration are commonly used [9, 10].

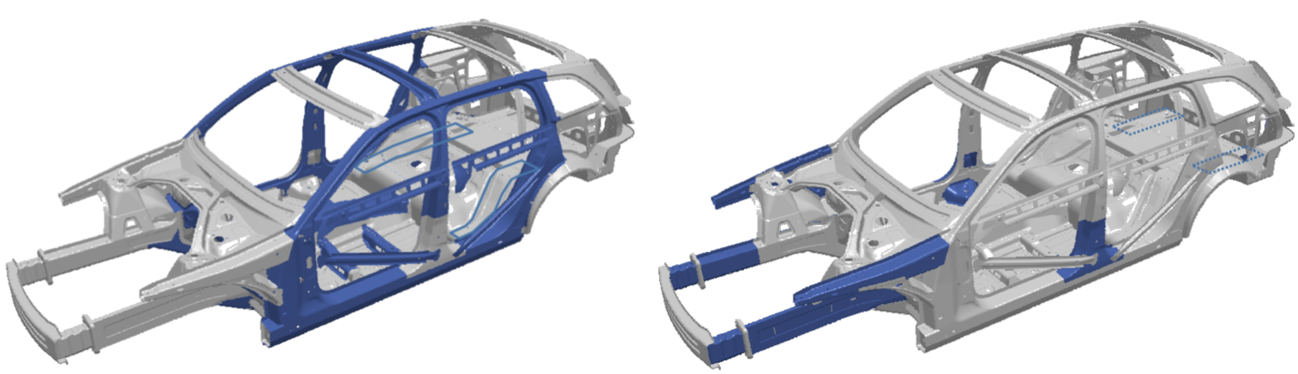

(a) Deformation resistance parts (blue)

(b) Energy absorbing parts (blue)

Figure 1: Example of a car body highlighting deformation resistance (left) and energy absorbing parts (right) for a frontal impact [11]

1.1. Simulation based car body development

The development of the car body structure is a highly complex task, where all components interact and the required force-deformation behaviour of the components is completely interdependent. Even the design of a single component is highly complex due to the high non-linear behaviour in terms of mechanical plasticity, failure, contact, buckling, large deformations, strain- and stress-rate-dependencies. In addition, a high number of different materials have to be modelled, ranging from different steel types and other metals to glass, polymers, foams, composites and bio-materials. The related computational effort is high; standard simulations take several hours and in some cases even days, despite the integration of high performance computing (HPC) in the simulation workflows. Therefore, to reduce this computational cost for the structural design of energy absorbing components there are two main approaches found in crash related literature, which are listed below and are illustrated in Figure 2.

a) **Full vehicle FEM simulations** with models as shown exemplarily in Figure 2: the complete structure of the car is modelled and the developer modifies a component (or components) assessing the changes via a complete repeat of the full set of crash simulations (note that a small change will affect the car performance in multiple different crash tests).

b) **Component simulations** with pre-defined boundary and initial conditions. For this, there are three options:

   b1) The energy absorption of a component is assessed under drop test conditions, i.e., a rigid plate or block with a certain mass and initial velocity is hitting the component. Here, the dynamic effects are covered more correctly.

   b2) A similar configuration as for b1) is used but by a crush test where a rigid wall with a prescribed and constant velocity deforms the component in axial direction. Because this is often done in a quasi-static manner, dynamic effects like inertia forces and (strain-)rate dependencies are neglected.

   b3) An alternative can be realised by using a full vehicle simulation and by registering the deformation- or velocity-over-time of the FE nodes at the interface between the component and the complete car structure. Then, the data of the interface nodes is used as constraints in the component simulations.

In some cases, a full-vehicle simulation is used to assess the performance of a single component. The advantage of this approach is that it takes all surrounding parts, as well as their interaction with the component, into account. However, especially during early stages of the development process, properties or design details of neighbouring components are not fully known. Typically, the development is a concurrent process between multiple designers or even departments / companies, where each designer or department is designing an individual component in parallel with activities of the others. Therefore, the full vehicle model at this point may not be available, under construction, or far from the final version. Hence, having a complete vehicle simulation during development may mean that pseudo-accuracy is introduced by the level of detail that is obtained, which neglects the development of other components. Therefore, potential wrong conclusions are made and redesigns at a later stage would be needed to correct for these decisions.

In addition, the potentially high computational effort of a full-vehicle simulation makes it nearly infeasible to realise a high number of full model simulations, such as needed for optimisation and robustness or reliability assessments. For instance, a single simulation of the Honda Accord model with 1.9 million elements [12] takes 14 hours on eight Intel(R) Core i9-7980XE CPUs. The academic example used in this work on the other hand, as illustrated in case a) in Figure 2, requires several minutes to calculate. Moreover, as the full car model consists of multiple

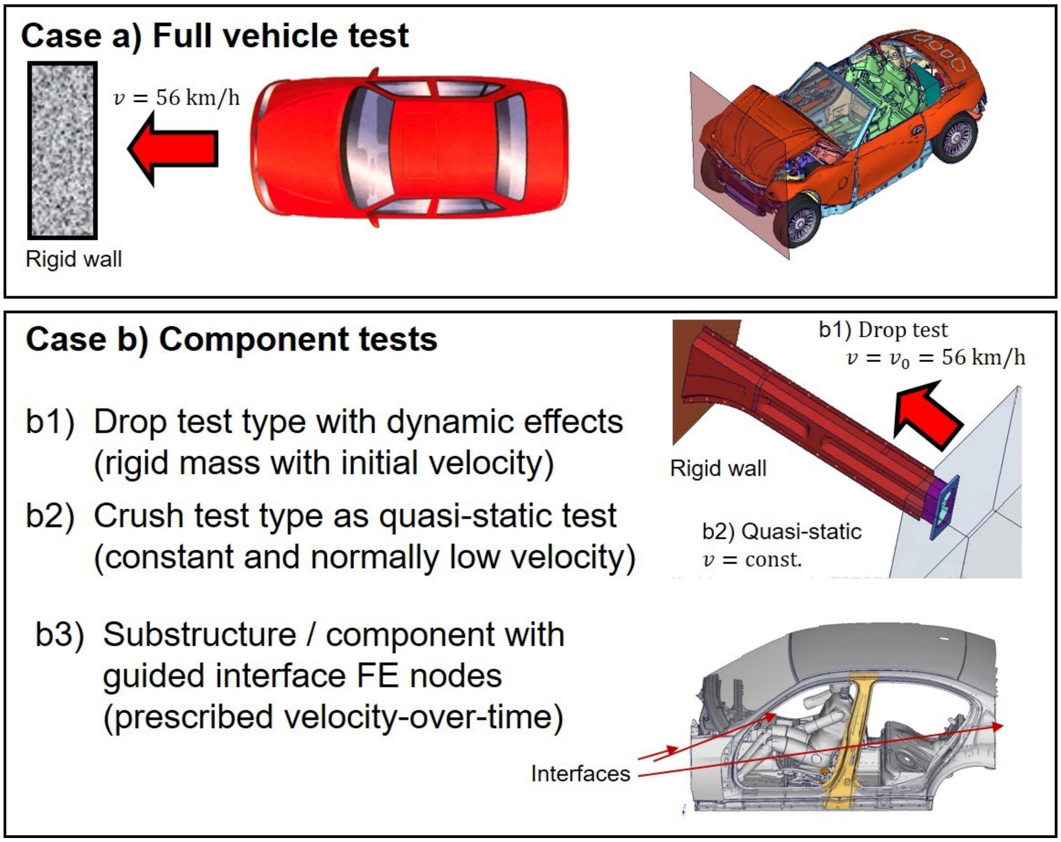

Figure 2: Example of full vehicle test (top) and component / sub-structure tests (bottom), after [4]

parts and materials that interact with each other, the uncertainties about all these parameters should be carefully assessed and quantified. Therefore, detailed investigations should be conducted concerning the range of these parameters as well as the relative likelihood of certain parameter values within this range (as commonly quantified by a distribution function). This is very challenging in general, and especially in an early design stage where many design decisions may still be open. In recent years, robustness studies on full vehicle models have been realised in, e.g., [5, 13]. However, these are rarely embedded in an industrial development and more importantly, the uncertainties considered are far from complete.

1.2. Uncertainty in crashworthiness

In the three versions of crashworthiness assessment of a single component illustrated in Figure 2, the parts are evaluated in an isolated environment neglecting the influence of possible modifications in the other components. However, from experience, we know that the mechanical response of other components strongly influences the behaviour of the component under consideration in the design study. Therefore, to the opinion of the authors, this - often unknown - difference between fixed boundary conditions and coupled boundary conditions to adjacent parts is of very high relevance, and should be considered in a single component impact performance optimisation under uncertainty. When neglected, the identified optimum may be of questionable value, as robustness or reliability problems on component level may lead to critical performance issues in the global crash performance of the complete vehicle. The advantage of the single component assessment is clearly the computational cost, i.e., a single assessment can be conducted at a fraction of the time it would take to run a full crash model. In addition, validation of these simulations via physical experiments is less complicated as drop-tower tests or quasi-static tests are widely used for single component testing, as opposed to full vehicle tests. The number of scientific papers on the assessment of components is very high, see [14, 15] to give only some of the most recent papers. However, the consideration of uncertainties is rarely undertaken on component level. As an example the reader is referred to [16].

Nevertheless, a range of methods is proposed in recent crash related literature that take these uncertain input parameters into account. Examples include load case and geometrical uncertainties [17, 13], or material uncertainties [18]. In these approaches, variations of the impact angles, locations and velocities are considered. In some cases, these quantities are also combined with the influence of manufacturing tolerances (variations in thickness, material parameters or geometrical features like radii) [4]. Following these numerical approaches, one typically assumes the uncertain input parameters to be independent. Regarding the parameters mentioned above, most of them are direct input parameters of the finite element model except the geometrical changes such as radii. For the latter, parametric shape modelling and mesh morphing tools have been developed [4]. In addition, efforts have been made on reducing the computational cost of uncertainty propagation by a multi-fidelity approach in [19], or adaptive Kriging based approaches in [20].

1.3. Complexity of hierarchical development

The application of optimisation with robustness and reliability analyses in an industrial setting remains challenging and time consuming, not only because of the high numerical effort. The main reason is related to the context of systems engineering and the necessity of hierarchical development caused by the high complexity of the product. This means that the different crash types (e.g. front, side, and rear impacts) are treated by different people or even departments and companies. As a consequence, every developer is working on a single component and not on the complete vehicle. Therefore, requirements must be broken down to the component level. Consequently, assessments are done as well on single components rather than on the full vehicle or system. The well-known V-model approach and the more recently developed Component Solution Space methodology [21, 22] enable this hierarchical development. However, following the Component Solution Space approach, it is challenging to include the inter-dependencies of the different components during a crash. As in the original Component Solution Space approach [21], deterministic force-deformation curves are obtained for each of the components, with a range that is maximised for each component until constraints are violated, e.g., order of plastic deformation, or acceleration limits. However, in real incidents, impact angle, speed and impacting object are unknown and the occurring deformations and force levels are uncertain. To resolve this, Component Solution Space methods have been introduced that incorporate epistemic uncertainty: where [23] focuses on uncertainties in force levels and [24] on remaining uncertainties, i.e., deformation lengths, energy to be absorbed, critical acceleration limit. These methods provide bounds on the range in which the component is performing as well as information about the range of uncertainty allowed for by the adjacent structure.

To overcome the issues related to the decoupled development of complex interacting structures, this paper presents a novel method to consider the interactions of a single component with these adjacent structures. Typically, the design and optimisation of these single components are based on droptower tests, b1 in Figure 2, where one typically measures force and deformation of an impacting object on a fixed specimen or component. However, this paper proposes a novel way to design and optimise a single component by introducing uncertain boundary conditions that account for the unknown behaviour of the adjacent structure, which is neglected in the typical tests. Nevertheless, from experience, we know that the mechanical response of other components strongly influences the behaviour of the component under consideration in the design study. Therefore, to the opinion of the authors, this - often unknown - difference between fixed boundary conditions and coupled boundary conditions to adjacent parts is of very high relevance, and should be considered in a single component impact performance optimisation under uncertainty. The structure of this paper is as follows: Section 2 gives a detailed description of the proposed implementation of interval fields at the boundary conditions. The difference between deterministic and uncertain boundary conditions is illustrated for a number of case studies in Section 3, followed by a discussion of the results in Section 4. Final conclusions are drawn in Section 5, which also provides an outlook of future challenges.

2. Non-deterministic modelling of the adjacent structure

The uncertainty in the proposed modelling strategy stems from the assumptions and abstractions that are made concerning the mechanical behaviour of the adjacent components. Since this uncertainty stems from a lack-of-knowledge about the final components, it is an attribute of the analysis, and hence, epistemic in nature. Therefore, it is proposed to model it using the interval framework. For the sake of argumentation, when one would attempt to model this type of uncertainty using probabilistic methods, subjective information is inserted into the analysis [25], which might give a false sense of accuracy. Applying interval analysis therefore is the most objective approach since it acknowledges that there is no information on the likelihood of relative parameter values within the interval bounds. Furthermore, when limited data about the actual boundary conditions are available, approaches to infer the bounds based either on Bayesian analysis [26] or inverse analysis can be applied [27].

A particular convenient interval technique for parameters that are spatially distributed is the recently introduced framework of interval fields, which can be regarded as a possibilistic counterpart to random fields [28] for quantities that are spatial or time dependent [29]. Following this framework of interval fields, locally defined intervals are expanded through the model domain based on a set of a priori defined basis functions. Multiple definitions of these basis functions can be found in literature, which are based on inverse distance weighting [27], affine arithmetic [30, 31, 32], radial basis functions [33], a spatial averaging method [34], or set-theoretical approaches [35, 36]. A recent overview of interval fields can be found in [25]. The following sections start with a detailed description of the interval field framework, and end with a description how this concept is used to model the epistemic uncertainty about the adjacent structure in a component finite element simulation.

2.1. Interval field analysis

This section provides a detailed description of interval field analysis, as introduced in [29]. In this work, the following definitions are used: interval parameters are indicated using apex I: x^I; a vector is indicated as lower-case boldface characters $\mathbf{x}$; matrices are expressed as upper-case boldface characters $\mathbf{X}$, and interval parameters are represented using the bounds of the interval defined as:

$$x^I = [\underline{x}; \overline{x}] = \{x \in \mathbb{R} \mid \underline{x} \leq x \leq \overline{x}\}, \tag{1}$$

where $\underline{x}$ stands for the lower bound and $\overline{x}$ for the upper bound. In addition, an interval can be represented by the centre point $\hat{x} = \frac{\underline{x}+\overline{x}}{2}$ and radius $\Delta x = \frac{\overline{x}-\underline{x}}{2}$ of the interval. An interval is considered *closed* when both the upper and lower bounds are a member of the interval. The domain of a real-valued interval is denoted as $\mathbb{IR}$.

2.1.1. Explicit interval fields

The definition of an explicit interval field is given in Equation (2), where the field consists of a superposition of $n_b \in \mathbb{N}$ base functions $\psi_i(\mathbf{r}) : \Omega \mapsto \mathbb{R}$ defined over the geometrical domain $\Omega \subset \mathbb{R}^d$, where d is defined as the physical dimension of the problem. These base functions describe the spatial nature of the uncertain parameter x, distributed along the coordinate $\mathbf{r} \in \Omega$. An interval field scales these basis functions $\psi(\mathbf{r})$ with independent interval scalars $\alpha_i^I \in \mathbb{IR}$, formally defined as:

$$x^I(\mathbf{r}) = \hat{x}(\mathbf{r}) + \sum_{i=1}^{n_b} \psi_i(\mathbf{r})\alpha_i^I. \tag{2}$$

with $\hat{x}(\mathbf{r}) \in \mathbb{R}$ the midpoint function of the interval field.

When Ω is discretised into n_e finite elements $\Omega^e \subseteq \Omega$, these base functions $\psi_i(\mathbf{r})$ interpolate the independent interval scalars α_i^I to dependent intervals for each $\Omega_i^e,\ i = 1, \ldots, n_e$ by projecting them onto a non-orthogonal vector space [37]. Further, the input space dimension is reduced if $n_b < n_e$, which reduces the computational cost of propagating the interval uncertainty towards bounds on the response quantity of interest.

2.1.2. Interval Field finite element analysis

Let $\mathcal{M}(\mathbf{x})$ be the deterministic model that represents the crash situation under consideration. The parameters of $\mathcal{M}$ are represented as a vector $\mathbf{x} \in \mathbb{R}^{n_x}$. The entries of $\mathbf{x}$ represent for instance constitutive material parameters, inertial moments or clamping stiffness. Solving the numerical model $\mathcal{M}$ corresponds to transforming the parameter vector $\mathbf{x}$ through a set of scalar function operators $m_i : \mathbb{R}^{n_x} \mapsto \mathbb{R},\ i = 1, \ldots, n_y$ to a vector of responses $\mathbf{y}(\mathbf{r}) \in \mathbb{R}^{n_y}$, defined as:

$$\mathcal{M} : \mathbf{y}(\mathbf{r}) = m_i(\mathbf{x}(\mathbf{r})) \quad i = 1, \ldots, n_y. \tag{3}$$

In an interval context, the uncertainty on $\mathbf{x}$ is represented as an interval vector $\mathbf{x}^I = [x_1^I, x_2^I, \ldots, x_{n_x}^I]$, with $x_i^I,\ i, \ldots, n_x$ the i^{th} parameter interval. It should be noted that $\mathbf{x}^I$ is constructed as the n_x-dimensional Cartesian product $\bigtimes_{i=1}^{n_x} x_i^I$, and hence, represents an n_x-dimensional hyper-rectangle. In the following, we consider the specific case where a single parameter of $\mathcal{M}$ is represented using an interval field $x^I(\mathbf{r})$. Hence, in this case, the input space is defined by the hyper-rectangle α^I. Note that this does not affect the generality of the developments, as the discussion can straightforwardly be extended towards multiple interval fields and/or combinations of interval fields and scalar intervals.

The main goal of the interval field analysis is to identify the set of system responses $\tilde{\mathbf{y}}$ that bounds the possible range of the responses $\mathbf{y}$ given $x^I(\mathbf{r})$. Since finding the exact set is in general computationally intractable, the exact solution set $\tilde{\mathbf{y}}$ is usually approximated by a realisation set $\tilde{\mathbf{y}}_s$ defined as:

$$\tilde{\mathbf{y}}_s = \left\{\mathbf{y}_j | \mathbf{y}_j = m_i(\mathbf{x}_j(\mathbf{r})); \mathbf{x}_j(\mathbf{r}) \in \mathbf{x}^I(\mathbf{r}); j = 1, \ldots, n_q\right\}. \tag{4}$$

The set $\tilde{\mathbf{y}}_s$ is typically constructed by n_q deterministic solutions $\mathbf{y}_j = \mathcal{M}(\mathbf{x_j})$ of the numerical model, where $\mathbf{y}_j$ is a vector containing the n_y deterministic responses of the j^{th} solution. For each of these n_q solutions, the interval field realisations $\mathbf{x}_j(\mathbf{r})$ are generated by drawing a realisation from the interval scalars constituting the interval field. The main challenge herein is choosing $\mathbf{x}_j(\mathbf{r})$ such that $\tilde{\mathbf{y}}_s$ is a conservative approximation of $\tilde{\mathbf{y}}$.

One way to obtain such approximation is to follow an optimisation approach. Here, $\tilde{\mathbf{y}}$ is approximated by a conservative hyper-cube $\mathbf{y}^I = [y_1^I, y_2^I, \ldots, y_u^I]$, with $\tilde{\mathbf{y}} \subseteq \mathbf{Y}^I$. The corresponding optimisation problem is defined as:

$$\begin{aligned} \underline{y}_i &= \min_{x \in \mathbf{x}^I} m_i(\mathbf{x}) \quad i, \ldots, n_y, \\ \overline{y}_i &= \max_{x \in \mathbf{x}^I} m_i(\mathbf{x}) \quad i, \ldots, n_y, \end{aligned} \tag{5}$$

where $y_i^I = [\underline{y}_i; \overline{y}_i]$ is the i^{th} solution interval. When a global minimum or maximum is found through optimisation, the smallest hyper-cubic approximation of the solution set $\tilde{\mathbf{y}}_s$ is identified. However, it should be noted that the behaviour of the goal function with respect to the uncertain parameters is unpredictable in the case of strongly non-linear problems, as considered in this paper. This makes the computational effort highly problem dependent [38]. It can furthermore be noted that the selection of the most appropriate optimisation algorithm is fully case-dependent. For a recent review on interval field propagation methods, the reader is referred to [25].

In the specific case of crash analysis, the functional relationship between $\mathbf{x}$ and $\mathbf{y}$, as given by $\mathcal{M}$, is strongly not convex. Therefore, the analyst has to resort to global optimisation schemes to solve Eq. 5. A particularly well-known non-gradient based algorithm is differential evolution (DE) [39], which is based on randomly selected sample points within the search domain. The parameters governing the optimisation are the population size, the mutation constant, and the recombination constant, which govern the number of samples that are used for each generation and the amount of parameter space that is being explored, i.e., by additional samples, versus refined, i.e., the new sample point is close to previously good performing points. For more information about this approach, the reader is referred to [40].

2.1.3. Definition of the basis functions

An open question in the discussion in the preceding section on using interval fields to propagate spatially uncertain quantities through $\mathcal{M}$ is the definition of the basis functions $\psi_i(\mathbf{r})$ $, i, \ldots, n_b$. Realisations of the interval field as defined in Equation (1) are obtained through discretisation of the basis functions. In this paper, the basis functions are based on the intuitive Inverse Distance Weighing (IDW) framework, as studied in detail in this context in [37]. Basis functions $\psi_i(\mathbf{r})$ based on IDW model the spatial dependence of the interval scalars α^I proportional to the inverse distance from predefined locations $\mathbf{r}_i$, i.e., control points, throughout the model domain Ω. In practice, the interval field is discretised over $\mathbf{r}_k$, which corresponds for instance to the element centre points, Gauss integration points, or nodal locations of the FE model under consideration. In this approach, the basis functions are based on a set of normalised weight functions $w_i(\mathbf{r}) \in \Omega$. These functions are explicitly defined as:

$$\psi_i(\mathbf{r}) = \frac{w_i(\mathbf{r})}{\sum_{j=1}^{n_b} w_j(\mathbf{r})}, \tag{6}$$

with $i = 1, \ldots, n_b$. The weight functions w_i are inversely proportional with respect to a distance measure $d(\cdot)$. This distance is measured to all other coordinates in the domain. A weight function w_i is denoted as:

$$w_i(\mathbf{r}) = \frac{1}{[d(\mathbf{r}_i, \mathbf{r})]^p}, \tag{7}$$

with the power $p \in \mathbb{R}^+$ as a non-negative parameter that can be set by the analyst to influence the rate of decay from the control point $\mathbf{r}_i$.

2.2. Boundary conditions described by interval fields

The discussion in this paper is based on a full vehicle crash model and an exemplary component, here a generic crash box, to illustrate the principle ideas. Figure 3 illustrates this component and the typical simulation setup, where on the left the finite element model of the component is shown and on the right an illustration of the typical boundary conditions is given where the red crosses indicate the fixed nodes. The case that is considered in this work is a full-width overlap crash test of a passenger car driving against a rigid barrier at 56 km/h, in accordance with the corresponding NCAP test [2]. This type of test set-up is defined in several consumer and regulation tests and is commonly used in scientific studies.

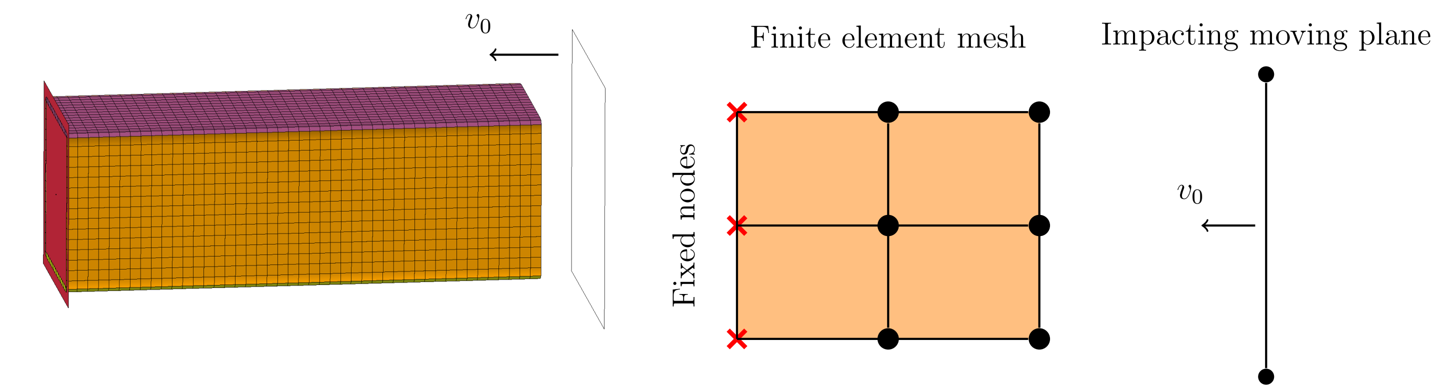

(a) Finite Element Model of the crashbox with a rigid plane attached to the nodes in the back (red) and impacting plane right

(b) Illustration of a general crash set-up, with the red crosses indicating the fixed nodes, and the impacting rigid plane on the right

Figure 3: Illustration of the crashbox and the general set-up of a crash analysis as used in this paper

The interval field concept is not directly applicable to this typical crash simulation, as illustrated in Figure 3b. First, a representation of the adjacent structure should be defined. In this case the adjacent structure is modelled at the back of the component between the rigid wall and the fixed nodes, which corresponds well to the physical location of these components within the vehicle. Figure 4 illustrates the adjacent structure modelled by a set of connecting elements. The epistemic uncertain lateral stiffness of these elements is represented by the interval field. Note, that the described method also works for elements placed in front of the component, or a combination of both, although this would require additional considerations about the properties of these elements.

2.2.1. Interval field modelling of the connecting elements

In this work, a novel technique is used to model a one-dimensional interval field on a three-dimensional component. This interval field is defined on the lateral stiffness of the elements connecting the crash-box to the surrounding. As such, the interval field models the uncertain compliance of the structure that is adjacent to the crash box. Specifically, the crash box is modelled as a rectangular shell that is meshed by two-dimensional shell elements. In this case, the nodes of the shell elements describe the circumference of a rectangular shape, as the thickness is considered in the shell formulation. Therefore, the distance measure used in IDW can be calculated along the circumference of the rectangular box, which yields a continuous one-dimensional interval field along the circumference of the component. However, since the vector $\mathbf{r}$ describes a position on a closed rectangular grid, the determination of the distance $d(\cdot)$ from the control point $\mathbf{r}_i$ to the other nodes $\mathbf{r}$ is less trivial as each nodal point can be reached following two distinct paths, i.e., clockwise, or counterclockwise. In this case, we consider the shortest distance between two

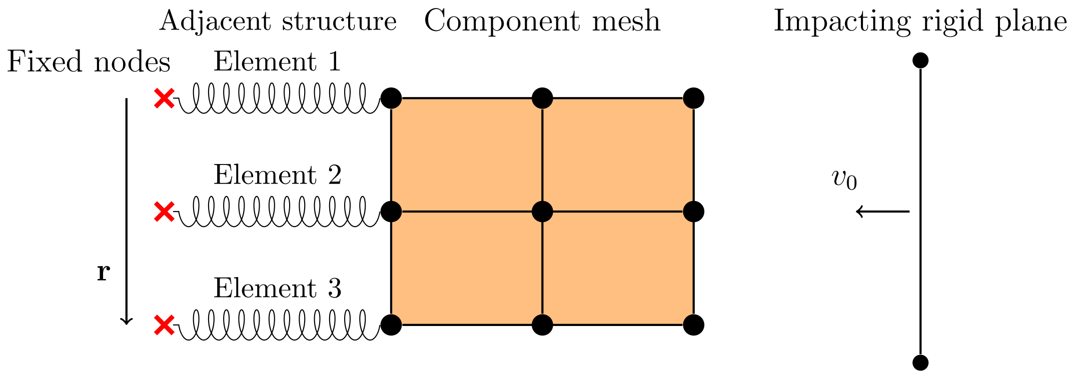

Figure 4: Illustration of the connecting elements, with the fixed nodes in red, the component in orange, and the rigid impacting plane on the right

points on the circumference. This can be solved by only using the shortest path between $\mathbf{r}_i$ and $\mathbf{r}$ to determine the distance measure. e.g., using Dijkstra shortest path algorithm [41]. In addition, element lengths can be directly used as weights in these shortest path algorithms and one directly obtains the distance. Note that the application of Dijkstra's algorithm in this case is superfluous since only two possible distances exist. However, in more general cases, multiple paths may exist. This motivates the application of shortest-path algorithms.

The other parameters to fully determine the interval field as described in Section 2.1 are: the power p, the interval scalars $\alpha_i^I,\ i,\dots n_b$, and the location of the control points $\mathbf{r}_i,\ i,\dots,n_b$. The influence of each of these parameters is described in detail in different case studies (see Section 3. In this paper, the power p is set at 2, which is reasonable based on prior experience [25]. It is interesting to point out that higher values of p will increase the weight of the closest control point and flatten the realisations near the control points, while a lower value of p decreases the influence of the control points where the realisation are all closer to an average value.

Two illustrations of realisations of the interval field are given in Figure 15, where the dashed black lines and red dots illustrate the variation of the normalised lateral stiffness of the elements towards the fixed wall nodes in blue. In addition, the control points $\mathbf{r}_i$ in this figure are shown as blue nodes with a black circle located at the coordinates $\mathbf{r}_i = [30, 30; 30, -30; -30, -30; -30, 30]$, and for some cases the control points are placed between the corner nodes located at the coordinates $\mathbf{r}_i = [2, 30; 30, -2; -2, -30; -30, 2]$.

2.2.2. Modelling the connecting elements

Depending on the analysis there are several ways to model the connecting elements at the back of the component. The appropriate selection of the element type is important, since it influences the energy balance of a crash simulation significantly. Figure 5 shows the effect of the connecting elements on the energy balance for two different material models. In a typical crash scenario, the kinetic energy E_k of the moving vehicle is fully translated into elastic and plastic deformation energy $E_d = E_{elastic} + E_{plastic}$, which is stored and dissipated by the deformation of the component. However, an additional energy storing and dissipation element is introduced by the introduction of the connecting elements. The amount of energy stored or dissipated in the elements depends on the interval field realisation and the material model that describes the behaviour of these elements. Figure 5b illustrates this behaviour where both, a linear and a bi-linear material model are shown by respectively the full and dashed lines. Here, the plastic deformation of the bi-linear model dissipates a part of the kinetic energy, which will therefore not be translated to the component. Therefore, the crash box is not subjected to the full kinetic energy of the impact. Such situation is undesirable as this biases the comparison of the dissipated energy in the crash box with respect to cases where less energy is dissipated in these connecting elements. Therefore, the connecting elements are modelled with a linear material behaviour. Further, such linear model also ensures a constant interaction between the component and the adjacent structure. The physical interpretation corresponds to a crash where a certain amount of energy is stored elastically within the complete structure, e.g., front structure of a vehicle, test machine, and this energy is released back from the most rigid components to the deformed components. However, note that when the elements are modelled as linear elastic elements, i.e., beams, forces higher than the yield force of the material can be reached for a short moment of time. Since the failure of these connecting elements are not of interest for the analysis, this is not critical.

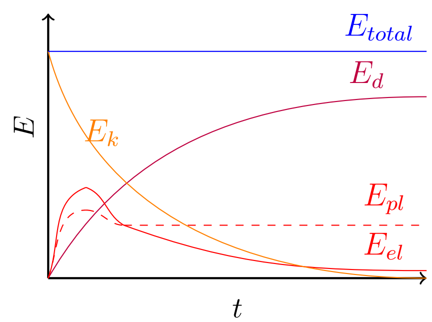

(a) Energy balance of one simulation where all the kinetic energy E_k is transformed into deformation energy E_d, and energy in the springs E_s;

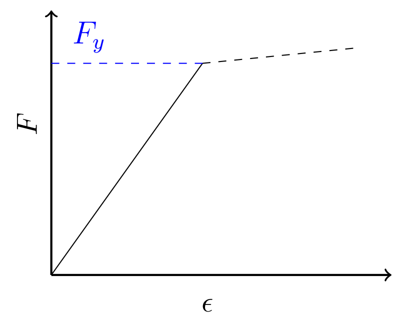

(b) Illustration of the stress-strain behaviour of different material models. Note that a little energy is lost in hourglass modes E_h, while the total energy remains constant

Figure 5: Two figures illustrating the impact of different material models on the energy balance of an impact simulation; indicated by the full and dashed lines

3. Case studies

In this section, four different approaches to model the lack-of-knowledge uncertainty about the adjacent structure are illustrated on a generic crash example. Specifically, the lateral stiffness of the linear connecting elements is modelled according to following approaches: (1) a deterministic benchmark case, (2) a scalar interval valued model, (3) an interval field approach, and finally (4) an interval field approach with a varying degree of uncertainty, modelled by changing the interval radius. The reasoning behind each of these cases is different where in the first cases (1-3) the main goal is to quantify the bound on the output given a certain degree of uncertainty, and the final case (4) is an investigation on the effect of different levels of uncertainty.

3.1. General setup and quantities of interest

In this section, a detailed investigation to the interactions between the interval field and a generic impact-critical component are conducted under a load case that is defined on the full overlap crash test. The generic component is represented by a rectangular box, which has sides of 60 mm, a total length of 180 mm with a thickness of 2 mm, which is modelled by 2700 four-node shell elements, as illustrated in Figure 3a. The properties of the sheet metal used for these components are modelled using a piece-wise linear plastic model [42]. The corresponding parameters are listed in Table 3.1. Following the load case, the component is impacted by a rigid moving wall with a mass of 60 kg. The initial velocity is set to 56 km/h or an equivalent 15.6 m/s. This provides a total kinetic energy of 7300.8 J at the start of the simulation. In engineering practice, it is common to assess the performance of these crash boxes in terms of the peak force and the mean force that are generated during impact. The goal of a general engineering design optimisation for impact is to identify the input parameters, such that an acceptable performance threshold is met. Conventionally, in crash analysis the goal is to achieve a force that is as constant as possible during the deformation.

Material model properties used for the component					
Mass density	ρ	7830 kg/m^3	Strain-rate parameter	P	5
Young's modulus	E	200 GPa	Strain-rate parameter	C	40
Poisson ratio	ν	0.3	Yield stress	σ_0	366 MPa
Equivalent stress	σ_1	424 MPa	Equivalent strain	e_1	0.025
Equivalent stress	σ_2	476 MPa	Equivalent strain	e_2	0.049
Equivalent stress	σ_3	507 MPa	Equivalent strain	e_3	0.072
Equivalent stress	σ_4	529 MPa	Equivalent strain	e_4	0.095
Equivalent stress	σ_5	546 MPa	Equivalent strain	e_5	0.118
Equivalent stress	σ_6	559 MPa	Equivalent strain	e_6	0.14
Equivalent stress	σ_7	584 MPa	Equivalent strain	e_7	0.182

Table 1: Material properties used in the piece-wise linear plasticity material model of the component

3.1.1. Peak force

The peak force is a measurement of the highest force that occurs during the impact simulation. In all considered cases, the peak force is measured at the rigid plane located at the back of the springs. The location is also indicated as a red plane in Figure 7. The peak force is measured directly from the output data without using any additional filtering:

$$F_{\text{peak}} = \max_{t \in \Delta t} F(t) \tag{8}$$

This causes this measurement to be noisy due to numerical instability of the explicit solution scheme. Typically, the peak force is measured just after the component and the rigid wall make contact, which initiates the start of the typical deformation folds. In general, high peak forces are avoided by car manufacturers as these are associated with high accelerations, which impose high forces on the adjacent structure and eventually the passengers leading to more severe injuries.

3.1.2. Mean force

The mean force is an average measurement of the force during impact and provides global information about the performance of a particular design. The mean force is calculated following Equation (9) where the total energy of the component E_{comp} is divided by the average final deformation $D(t_{\text{final}})$. In order to omit zero entries, only the force and deformation starting from impact until the kinetic energy is zero are considered $t_{\text{final}} : E_{\text{kinetic}}(t_{\text{final}}) = 0$, neglecting the elastic spring-back of the component.

$$F_{\text{mean}} = \frac{E_{\text{comp}}(t_{\text{final}})}{D(t_{\text{final}})}, \tag{9}$$

where $D(t_{\text{final}})$ is calculated as the average displacement between the nodes of the start and the end of the crash box.

3.2. Benchmark case

This first case is used as a benchmark where the boundary conditions are applied in a normal way, with two rigid planes in correspondence with the illustration in Figure 3b. Therefore, only a single simulation is performed as there are no uncertainties considered in this case. The result of this simulation is provided by means of a force-displacement graph, shown in Figure 6. In this graph, the peak force and mean force measurements are indicated by a blue dot and an orange dashed line, respectively. Note that it is common within industry to filter the results of the numerical simulations of crash scenarios, see e.g., [43]. However, as there are no experimental data to compare to, the results shown in this paper are provided without the use of any filtering. It is clear that there is a large difference in peak force and mean force, which is not unexpected for a component with this geometry, which is not optimised in any sense. In an industrial environment, one would typically optimise the component such that the peak and mean force are more or less equal to each other, or below an a priori set threshold.

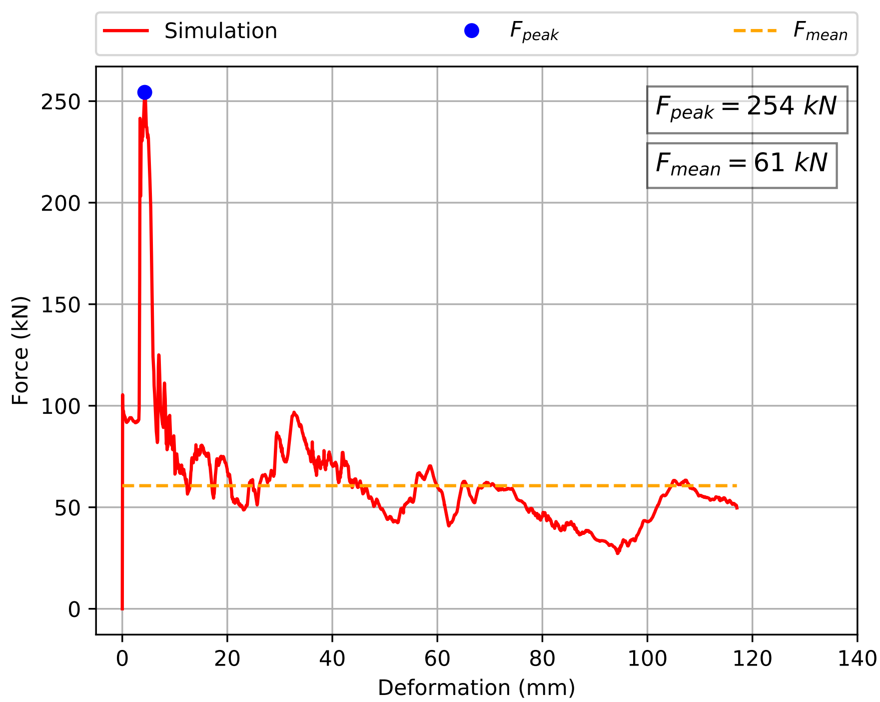

Figure 6: Force-deformation curve of the benchmark case without filtering, red; location of the peak force, blue dot; and the mean force, orange dashed line

The multiple peaks that are seen in Figure 6 are located at times where the force has built up until reaching a threshold before the next fold is initiated. This corresponds perfectly with the observed folding pattern, as illustrated in Figure 7. In this figure, the red plane is fixed and the white plane on the right is impacting the structure, in correspondence with Figure 3b. The folding pattern shows that three folds are created during the first 12 ms of the impact, which is a local buckling mode starting at the impacting plane. The computational time for this simulation is approximately 2 minutes on two cores of an Intel(R) Xeon(R) CPU E5-2695 v3 @ 2.3GHz processor, which is reasonable in comparison to performing simulations on a full vehicle model.

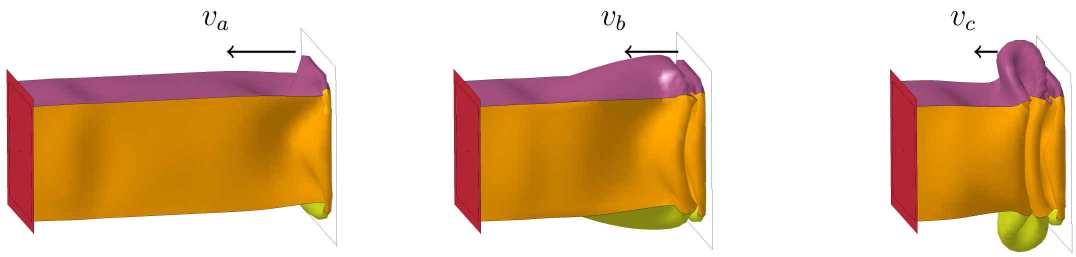

(a) time = 3 ms (b) time = 6.5 ms (c) time = 12 ms

Figure 7: Deformation of the benchmark case with fixed boundary conditions at different time steps, with the fixed plane in red, and the impacting plane in white

3.3. Interval valued non-deterministic modelling of the adjacent structure

In the following case studies, the non-deterministic effects of the adjacent structure are modelled by a set of springs at the back of the component. These springs are illustrated in Figure 4. The lateral stiffness of each element is determined following a discretisation of the interval field. This interval field with IDW basis functions is used to model the spatial dependency of the element stiffness, which corresponds to the physical reality where the point-wise deformation of two points in an adjacent component is also dependent on the neighbouring areas in this component. As such, the interval field models the spatial distribution that is in a full-scale analysis provided by adjacent connecting elements. Additionally, it is shown that it is needed to optimise the input parameters of the interval field to obtain the worst case response of the structure, i.e., a response that results in structural failure defined as higher accelerations.

3.3.1. Interval valued stiffness of the adjacent structure

For this case, the bounds of the lateral stiffness interval are considered to be given as $k_t^I = [200;\ 330]$ MPa. Furthermore, it is assumed that all elements take the same stiffness value. This assumption will not provide the worst-case bounds on the response as this would require the use of optimisation, which is used in general for non-monotonic problems [44, 45], and as will be applied in the latter case studies in this paper. Nonetheless, the analysis is performed with these assumptions to illustrate the effect the elements have on the overall performance of the crashbox. The results of this case study are illustrated in Figure 8. In this figure, the force deformation curves of this case are compared with those of the benchmark case. Figure 8 shows that both the obtained mean force as well as the peak forces are lower than those of the benchmark case, by 5.4 kN and 15 kN respectively. In addition, it also shows that the peak force is reached at a lower deformation in both cases. This behaviour is explained by the elements that absorb, and therefore deform, a part of the kinetic energy especially at the start of the impact, which is shown in Figure 9. This figure shows that the time to absorb the kinetic energy is both higher and lower depending whether the lower or upper bound is used. Hence, the time to build up the force and initiate the first folds is increased.

Figure 9 shows that in the final stages of the impact event the elements set at the lower value of the stiffness accumulate more energy than the stiffer elements (indicated in red), which causes the total kinetic energy to be absorbed sooner. Therefore, the elements influence the time in which the kinetic energy is absorbed by the component and the amount of kinetic energy, as a part remains within the elements. The latter is of course an undesired effect as these components are designed to dissipate a certain amount of kinetic energy. Therefore, care should be taken to

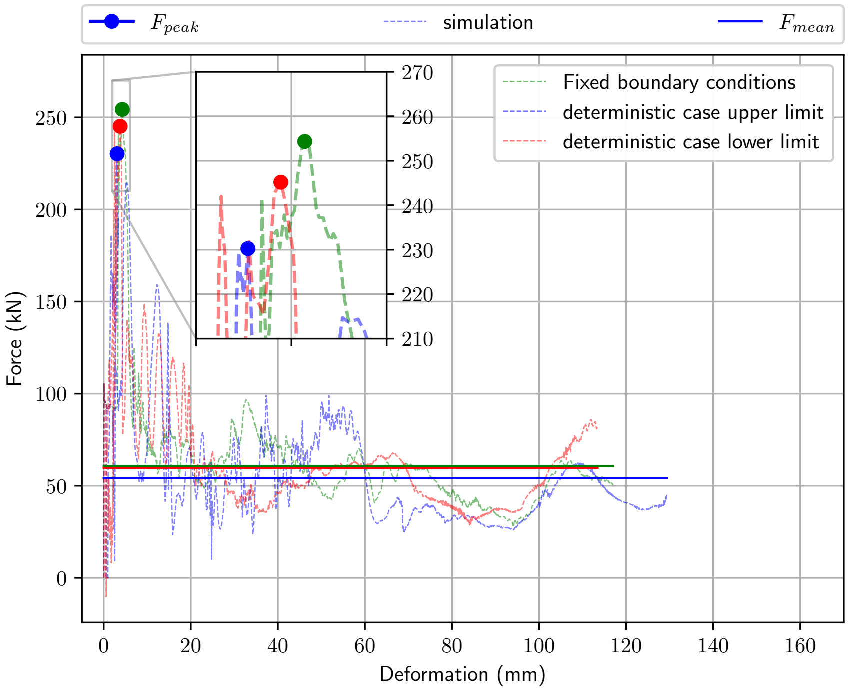

Figure 8: Force-deformation curves of the interval valued case with the minimal and maximal peak- and mean force indicated by arrows and solid lines, in blue and red

limit the amount that is elastically stored within the springs. Moreover, this figure also shows the energy accumulated by the deformation of the component E_{comp}, the kinetic energy E_{kin}, hourglass energy E_{hg}, and the total energy E_{tot} of the simulation, which are truncated at the time all kinetic energy is dissipated.

Finally, Figure 10 illustrates the deformation pattern at specific time steps where the results of the upper row are set at the upper limit of the interval and the second row is set at the lower interval value. It is clear from this figure that the deformation in both runs is quite similar but with a small time delay for the lower limit, which is also less deformed at the end of the impact after 18 ms.

3.3.2. Interval valued spatial uncertain stiffness controlled at the corners

In this case study, the interval valued stiffness for the elements is assumed to be spatially coupled, while the size of the interval is identical to this of the previous case. As explained earlier, this corresponds to the physical presence of the adjacent structure. The stiffness values of the elements are coupled by means of an interval field. In this interval field, a set of discrete control points are placed at the corner nodes of the crashbox. Further, rather than modelling the stiffness of each of the 60 elements separately, only 4 parameters are required. This is advantageous from a computational standpoint. The interval field used in this case is defined in section 2.1 with basis functions that are based on IDW with $p = 2$, and the interval of the lateral stiffness is assumed to have a midpoint of $\hat{x} = 265$ MPa with a radius of $\Delta x = 65$ MPa, which corresponds to the interval used in previous case $k_t^I = [200;\ 330]$ MPa. The bounds of the response are in this case estimated by global optimisation using a differential evolution algorithm (DE). DE uses different populations for each generation within the input space to actively search for the global minimum. The results and the settings for the optimisation algorithm are summarised in Table 2, where the

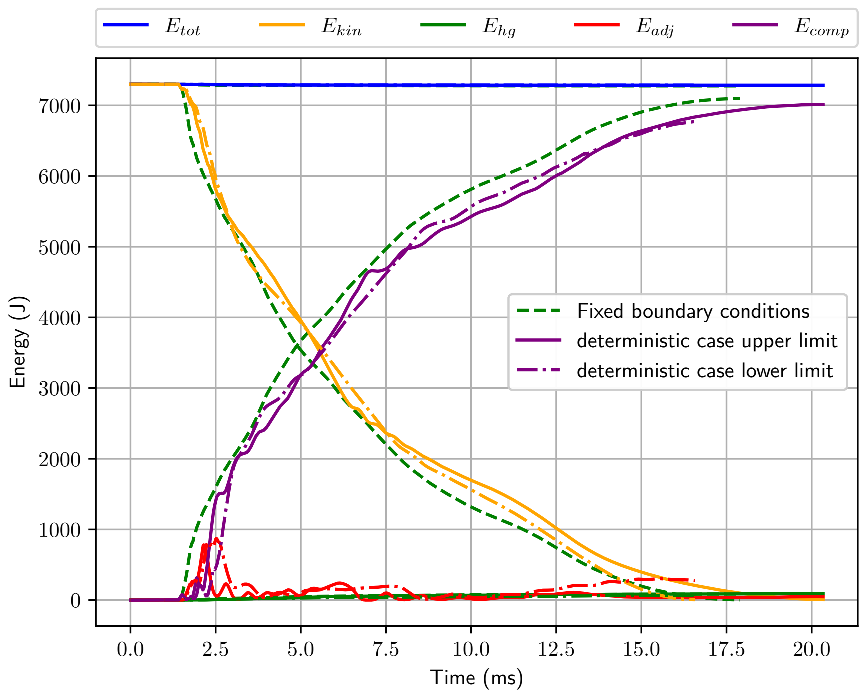

Figure 9: Energy balance of the interval valued case whit: the total energy E_{tot} blue, the kinetic energy E_{kin} yellow, hourglass energy E_{hg} green, the energy of the adjacent structure E_{adj} red, and the energy of the component E_{comp} purple

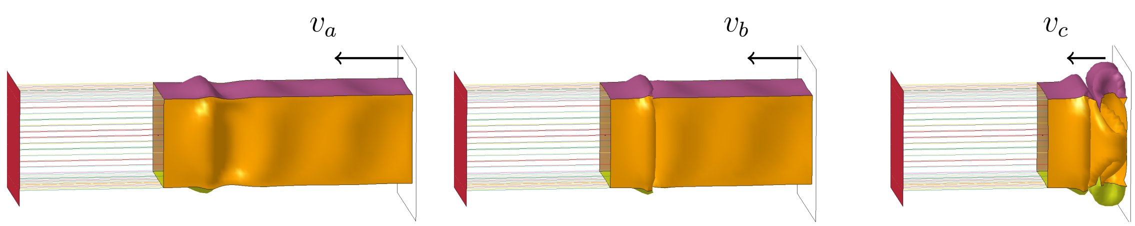

(a) time = 2.5 ms (b) time = 5 ms (c) time = 18 ms

Deformation obtained by propagation of upper limit

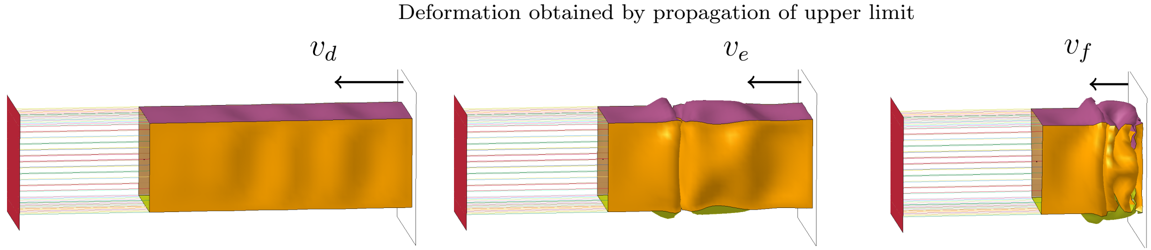

(d) time = 2.5 ms (e) time = 5 ms (f) time = 18 ms

Deformation obtained by propagation of lower limit

Figure 10: Deformation of the interval valued case at identical time steps, with the fixed plane in red, and the impacting plane in white

interval scalars are denoted with an $*$ when obtained through optimisation $\alpha^* = \max m_i(\mathbf{x}^I)$.

results of DE using control points at the corner nodes										
value	pop	rec	mut	nfal	nit	α_1^*	α_2^*	α_3^*	α_4^*	Optimisation
224.4	20	0.3	[0.9 1.7]	1155	56	0.0634	0.9663	0.1508	0.2748	min F_{peak}
261.7	20	0.3	[0.9 1.7]	220	8	0.4767	0.6706	0.6464	0.3902	max F_{peak}
42.2	20	0.3	[0.9 1.7]	1325	59	0.5267	0.9036	0.5703	0.0222	min F_{mean}
61.4	20	0.3	[0.9 1.7]	9850	257	0.7300	0.1332	0.8988	0.1077	max F_{mean}

Table 2: Results of the case study with control points at the corner nodes, including the DE parameters: population size (pop), recombination constant (rec), mutation constant (mut), with the number of evaluations (nfal) and iterations (nit) needed to identify the optimal interval scalar parameter α^* for the different optimisation runs

From the summary in Table 2 and the corresponding force-deformation curves in Figure 11, it is clear that when optimisation is used to actively search for the bounds, a larger interval is found for both, the mean force and the peak force. Especially in comparison with the previous case, it is clear that variation of the stiffness between elements yields larger bounds on the response for both quantities of interest. Figure 11 further illustrates that both the minimal mean force as well as the minimal peak force are very low in the region between 30 and 80 mm of deformation, before starting to increase again. The cause of this effect can be seen in the deformation pattern in Figure 12, where it is clear that a global buckling mode is activated. This causes the crashbox to "fold" and lose its structural integrity. The force is only going up after 140 mm of deformation because the collapsed structure is still between the two rigid planes and is starting to get further compressed. Hence, it is argued that from this level of uncertainty realisations are possible where the performance of the component is no longer guaranteed, as the global buckling mode prevents the dissipation of the kinetic energy.

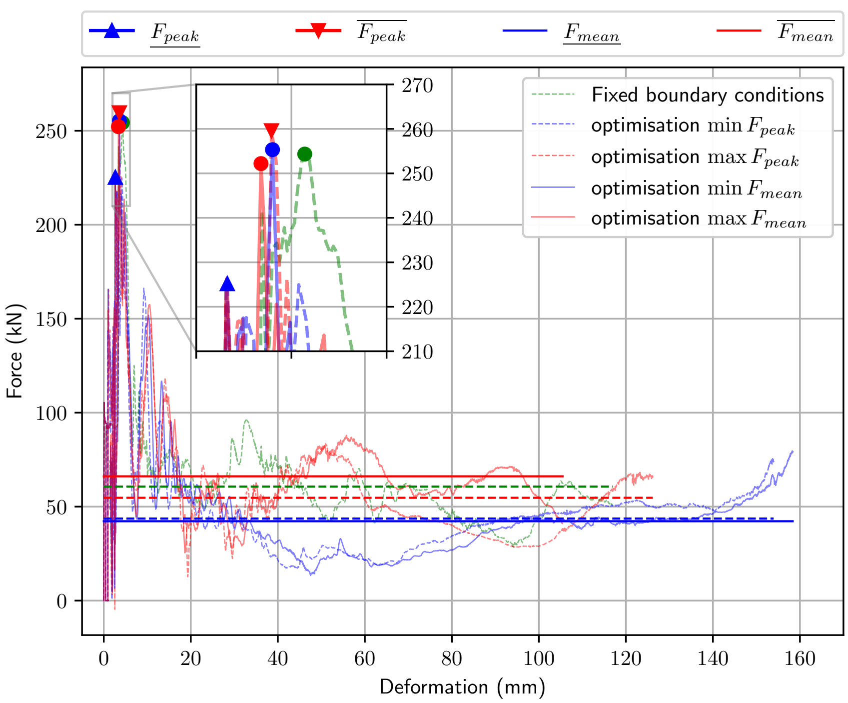

Figure 11: Force-deformation curves for the case with four control points at the corners obtained through optimisation; with the minimal and maximal peak- and mean force indicated by arrows and solid lines, in blue and red

Figure 11 also shows that the optimisation procedure yielded a mean force which is higher than the mean force that was obtained in the benchmark case. This is illustrated in green colour. The reason for a higher mean force is found in Figure 12. Based on this figure, the higher mean force is attributed to a more dense folding pattern. Because of this denser folding pattern, the total deformation of the crashbox is also shorter than for the benchmark case, which can also be seen in Figure 11. This indicates that, for an equal kinetic energy, interactions between the component and the adjacent structure can result in mean forces both higher and lower than these identified with the benchmark case.

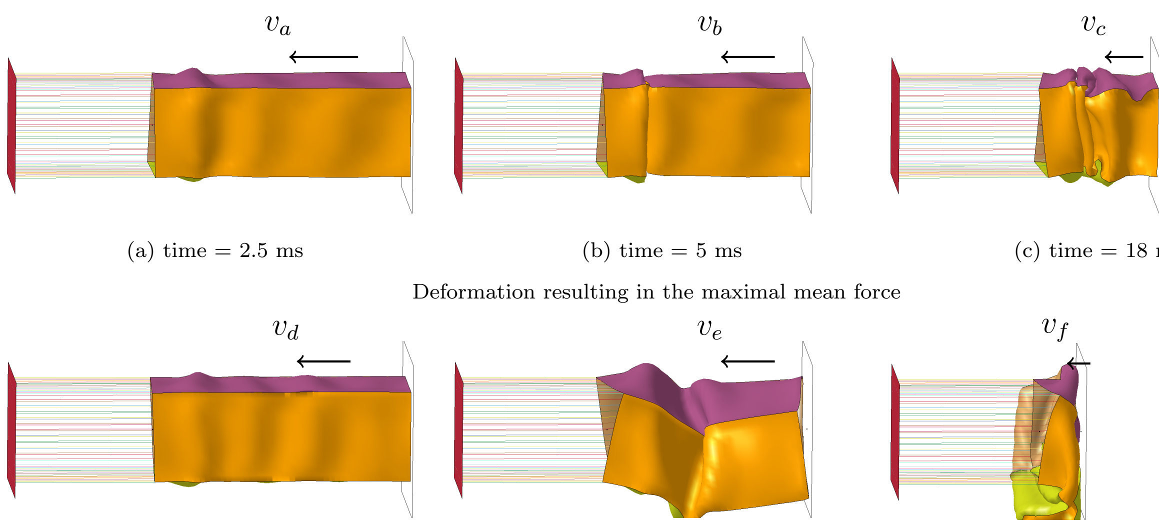

(a) time = 2.5 ms (b) time = 5 ms (c) time = 18 ms

Deformation resulting in the maximal mean force

(d) time = 2.5 ms (e) time = 5 ms (f) time = 18 ms

Deformation resulting in the minimal mean force

Figure 12: Deformation of the case with four control points at the corners at identical time steps, with the fixed plane in red, and the impacting plane in white

To gain a better understanding of these interactions, it is also useful to look at the realisations of the interval field. These realisations are illustrated in Figure 13 with the left hand realisation corresponding to the maximum peak force and the right hand configuration to the minimum mean force. The control points of the interval field are indicated by a black circle in this figure and the normalised stiffness of the elements is indicated by the relative length of the black dashed lines. It is clear from this figure that the global buckling mode is obtained by a realisation that resembles a plane which is placed at an angle, while the maximum mean force is obtained by making differences between opposite corners. These realisations are not only interesting from the point of uncertainty quantification as they can also assist in the way these components are manufactured and joined together, which initiates relative changes of stiffness.

3.3.3. Interval valued spatial uncertain stiffness controlled between the corner nodes

For this case, the locations of the control points are changed, which directly influences the possible realisations of the interval field. A summary of the results obtained through optimisation using a differential evolution algorithm is given in Table 3. In a comparison with the previous case it is noticed that there is a change in the upper limit of the peak force and the mean force, which indicates that this configuration allows for a different interaction with the elements.

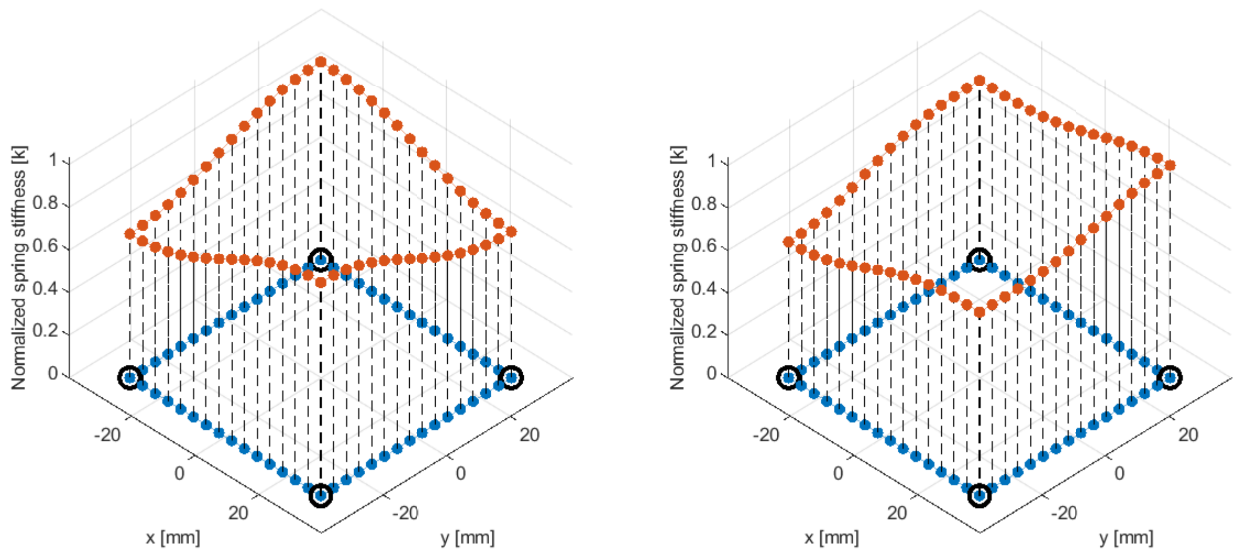

(a) Realisation of the interval field according to $\alpha^* = \max m_i(\mathbf{x}^I)$ (b) Realisation of the interval field according to $\alpha^* = \min m_i(\mathbf{x}^I)$

Figure 13: Realisations of the interval field with four control points, resulting in the minimal and maximum mean force; control points are indicated by a black circle and the length of the dashed line indicates the normalised stiffness value

results of DE using control points between the corner nodes										
value	pop	rec	mut	nfal	nit	α_1^*	α_2^*	α_3^*	α_4^*	Optimisation
224.3	20	0.3	[0.9 1.7]	1140	55	0.0391	0.2447	0.8808	0.3498	min F_{peak}
264.0	20	0.3	[0.9 1.7]	320	14	0.5126	0.7282	0.3702	0.6913	max F_{peak}
41.9	20	0.3	[0.9 1.7]	5125	250	0.3034	0.9278	0.9953	0.1621	min F_{mean}
62.8	20	0.3	[0.9 1.7]	975	44	0.5595	0.5065	0.9198	0.2090	max F_{mean}

Table 3: results of the case with control points between the corner nodes, including the DE parameters: population size(pop), recombination constant (rec), mutation constant (mut), with the number of evaluations (nfal) and iterations (nit) needed to identify the optimal interval scalar parameter α^* for the different optimisation runs

Figure 14 shows the deformation pattern that yielded the minimal and maximal mean force at different time steps. Compared to the previous case, these deformation patterns look quite different at a first glance, nevertheless when a closer look is taken it seems that these are more familiar to the previous cases, seen from a different viewpoint. This could be the case as the configuration of the interval field is not unique, which causes the component to buckle in a different direction when the control points are rotated. This is not true in general as in this case the box is a simple symmetric geometry, which is not true in the presence of holes and fold initiators.

In addition, the realisations of the interval field are provided in Figure 15 where the different location of the control points are indicated by the black circle. The non-uniqueness in this case can be seen as rotating the interval realisation by 90 degrees, which yields the same results. It is also visible in this figure that the minimal mean force is obtained by a similar realisation as seen in the previous case. For the maximal mean force a different realisation is responsible for the observed differences.

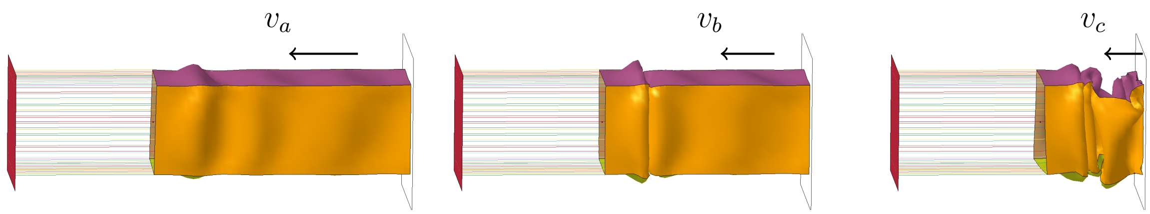

(a) time = 2.5 ms (b) time = 5 ms (c) time = 18 ms

Deformation resulting in the maximal mean force

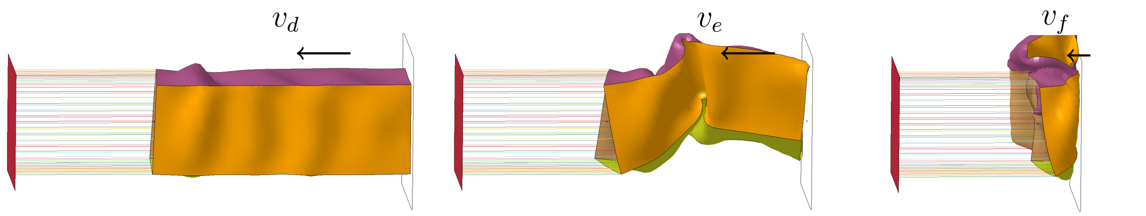

(d) time = 2.5 ms (e) time = 5 ms (f) time = 18 ms

Deformation resulting in the maximal mean force

Figure 14: Deformation of the case with four control points at the corners at identical time steps, with the fixed plane in red, and the impacting plane in white

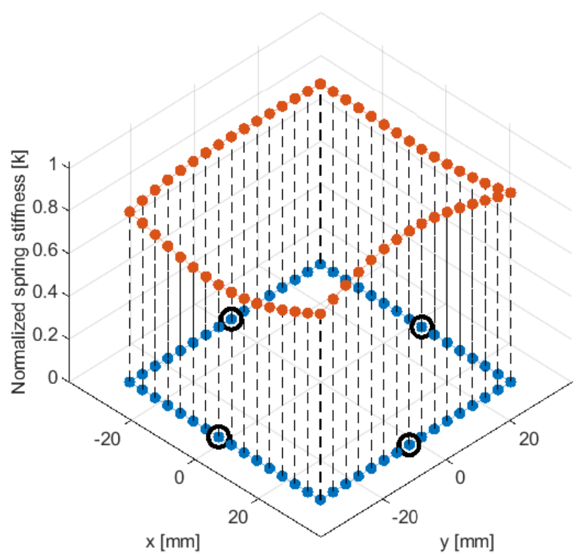

(a) Realisation of the interval field according to $\alpha^* = \max m_i(\mathbf{x}^I)$

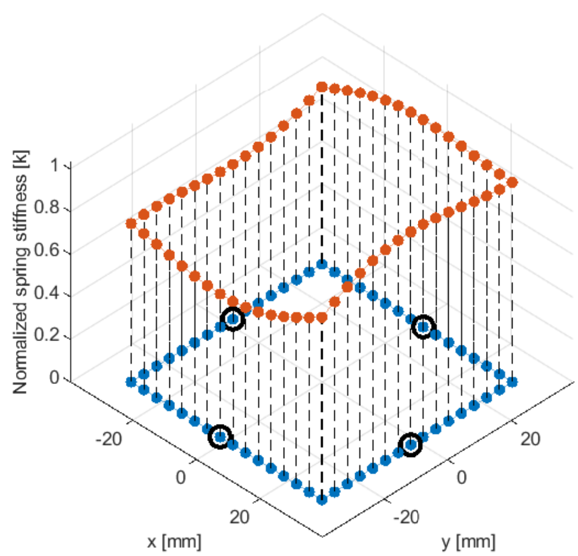

(b) Realisation of the interval field according to $\alpha^* = \min m_i(\mathbf{x}^I)$

Figure 15: Realisations of the interval field with four control points, resulting in the minimal and maximum mean force; control points are indicated by a black circle and the length of the dashed line indicates the normalised stiffness value

3.3.4. Increased degree of freedom by placing additional control points

In this case, the degrees of freedom of the interval field are increased by placing additional control points, which allows the realisations of the interval field to have a more complex shape. Hence, this case represents a combination of the previous cases constructed by placing control points at both, the corner nodes and between them. The results of this case are summarised in

Table 4, which indicates that in general the bounds on the response have increased.

results of DE using eight control points												
value	pop	nfal	nit	α_1^*	α_2^*	α_3^*	α_4^*	α_5^*	α_6^*	α_7^*	α_8^*	Optimisation
224.1	26	5652	350	0.08	0.05	0.79	0.55	0.65	0.68	0.19	0.02	min F_{peak}
263.4	26	864	32	0.25	0.85	0.33	0.55	0.66	0.59	0.46	0.89	max F_{peak}
41.3	26	5832	350	0.95	0.90	0.56	0.04	0.04	0.53	0.20	0.92	min F_{mean}
64.7	26	5831	350	0.53	0.67	0.05	0.96	0.46	0.26	0.98	0.35	max F_{mean}

Table 4: results of the case using eight control points, here the DE parameters: recombination constant (rec), mutation constant (mut) are identical to the previous case, while the population size(pop), number of evaluations (nfal) and iterations (nit) needed to identify the optimal interval scalar parameter α^* for the different optimisation runs are provided

These increasing bounds are expected as the additional control points increase the dimension of the input space, which also results in an increased time to perform the optimisation. It is noticed that the optimisation algorithm quickly identifies realisations that result in a high or low mean force, and starts optimising the elements to have the lowest stiffness that still initiates the global buckling mode. The mean reason is that after buckling of the component the moving rigid plane starts impacting the elements, which provide a lower force if they have a lower stiffness. This is observed by the fast increase in force in Figure 16 while the energy in the springs Figure 17 is not increasing. Hence, it can be argued that the component is not capable of dissipating all kinetic energy under this amount of uncertainty.

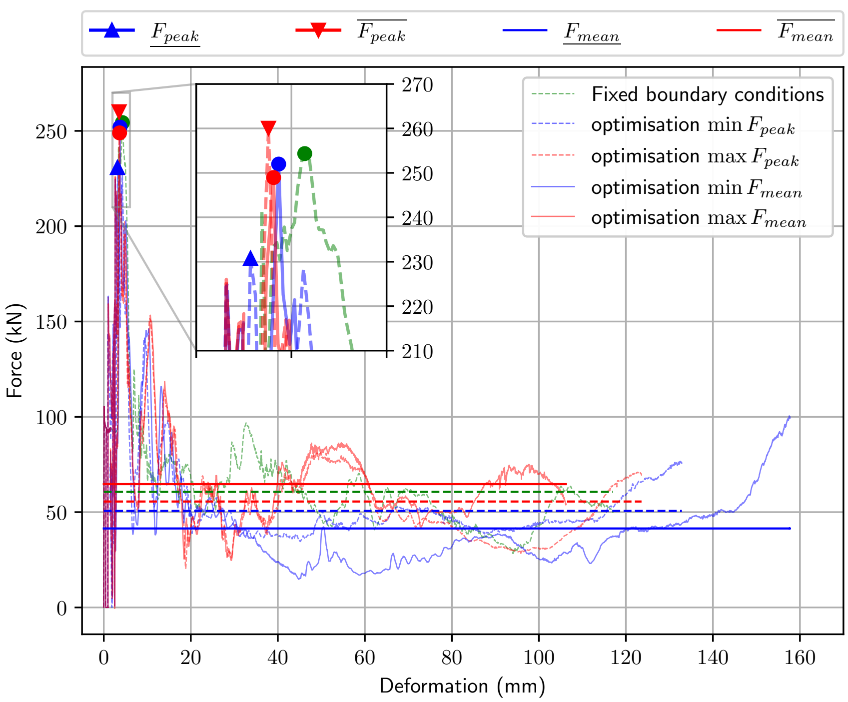

Figure 16: Force-deformation curves for the case with eight control points obtained through optimisation; with the minimal and maximal peak- and mean force indicated by arrows and solid lines, in blue and red

The realisations of the interval field with eight control points are shown in Figure 18b where the realisation yielding the maximum mean force is shown on the left and the minimal mean force

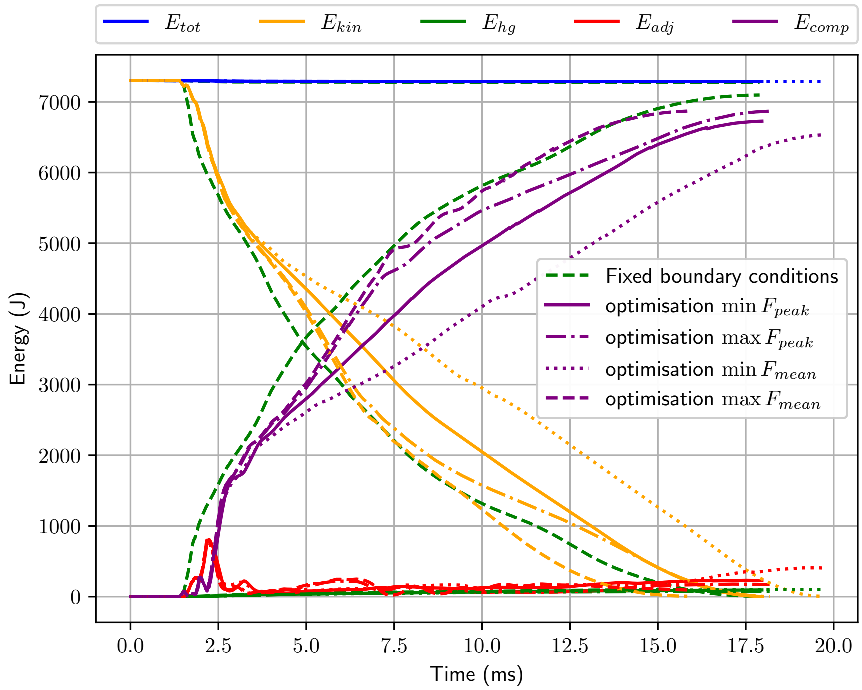

Figure 17: Energy balance of the interval valued case whit: the total energy E_{tot} blue, the kinetic energy E_{kin} yellow, hourglass energy E_{hg} green, the energy of the adjacent structure E_{adj} red, and the energy of the component E_{comp} purple

on the right. As in the previous cases, the realisation that yields the minimal mean force is quite similar and the maximum mean force is a result of a more complex interaction with the elements at the end of the component.

3.4. Interval field with increasing uncertainty

In this case the uncertainty in the interval field model, quantified by the width of the bounds, is varied by changing the radius of the interval Δx. This study is aimed at identifying the performance of the component under different levels of uncertainty. In this case, the level of uncertainty that allows to deform the component by a global buckling mode is of main concern as this prevents the component from fully dissipating the kinetic energy, which is the main purpose of this component. The corresponding level of uncertainty is identified by running a set of optimisations using the same settings as in Section 3.3.2 while the interval radius Δx is varied. The results of all these individual optimisations are provided in Figure 19 where each of the optimisation runs are identified by a marker for the upper and lower bound. Figure 19 shows that with an increase of the interval radius a non-monotonic increase of the bounds on the output, indicated in red and blue, is obtained. Especially the large step made by the lower bound of the mean force between $\Delta x = 32.5$ MPa and $\Delta x = 34.5$ MPa is of interest as this indicates the transition between a folding pattern towards the global buckling mode, which is regarded as a failure. This is also observed in the deformation patterns, in the same figure, at a single time step of 5 ms, which illustrate the transition in the observed deformation pattern. This information can be used in a component optimisation where a better design is performing better under a wider range of uncertainty, which would make it more robust. This robustness is not limited to the component alone as it translates to the complete structure, which will meet the requirements under a wider range of circumstances.

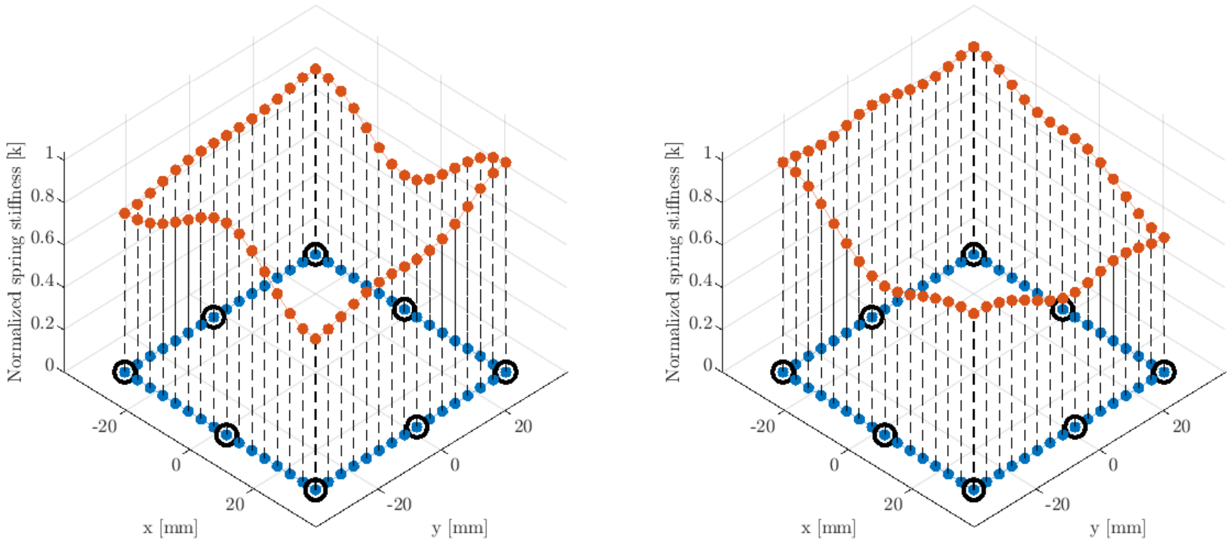

(a) Realisation of the interval field according to $\alpha^* = \max m_i(\mathbf{x}^I)$ (b) Realisation of the interval field according to $\alpha^* = \min m_i(\mathbf{x}^I)$

Figure 18: Realisations of the interval field with eight control points, resulting in the minimal and maximum mean force; control points are indicated by a black circle and the length of the dashed line indicates the normalised stiffness value

In addition, the markers in Figure 19 show that the DE algorithm was unable to identify the same minimum that was obtained in another optimisation run, which yields the adjusted bounds identified by a circle. The adjustments of the bound for each of these circles was about ten times smaller in absolute value compared to the step that is observed at the minimum mean force bound. Although, this step occurs at a seemingly arbitrary value of $\Delta x = 32.5$ MPa, the important lessons are the different worst-case deformation patterns that are occurring. Moreover, this value of Δx can be seen as a measure of the robustness of the component with respect to the uncertain input. Hence, the robustness is interpreted as the ability of the component to perform within certain limits for a range of uncertainty.

4. Discussion

In the previous section, a number of cases are shown starting from a benchmark case, an interval valued case, interval field analysis and finally an interval field approach with increasing uncertainty. These cases illustrate the use and additional value of using non-deterministic modelling strategies in crash simulation. However, a number of important findings are further elaborated on in this section that allow for a more general discussion about the results.

The first finding is that the elements at the back of the component are also dissipating kinetic energy, which is a direct result of the stiffness of each spring and the reaction force of the component. This effect is first shown in the benchmark case, Section 3.2, where at the start of the impact energy is stored at the springs, which is released later. Nevertheless, in Section 3.3.4 it is also shown that the optimisation algorithm converges to a configuration of the elements that ensures failure of the component while maximising the amount of elastic energy stored within the elements. This configuration leads to lowest mean force after the component lost structural rigidity, which can be interpreted as failure. Therefore, energy storage at the end of the impact

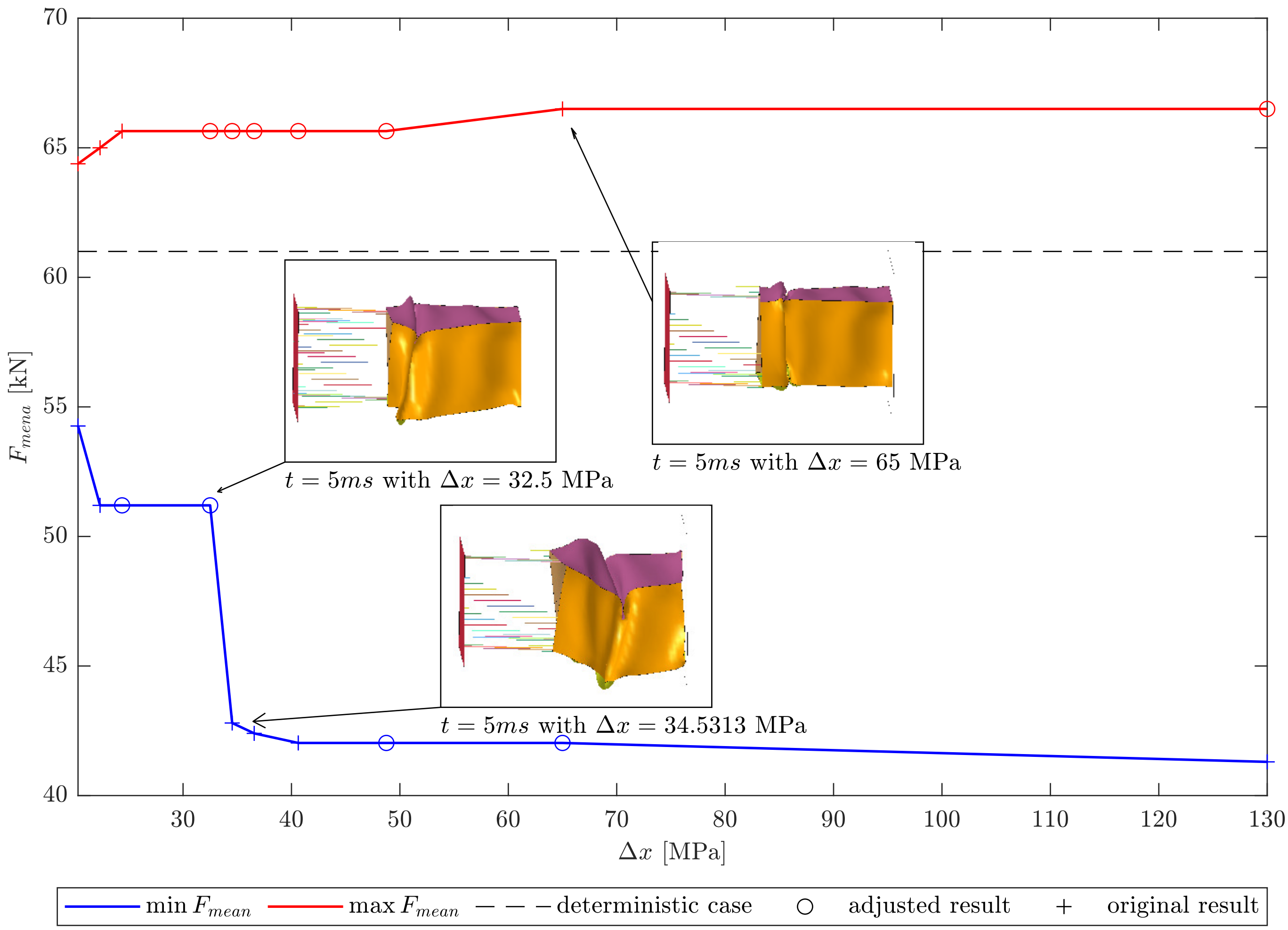

Figure 19: Bounds of the mean force identified through global optimisation for different values of interval radius Δx, with the corresponding deformation at identical times

event stored within these elements is undesired and should be limited or accounted for within the optimisation, as this limits the kinetic energy dissipated by the component.

The second point that stands out in this analysis is related to the optimisation algorithm that is used to obtain the bounds on the output quantities. It is noted that the DE algorithm experiences some difficulties to reach a converged solution for some of the optimisation runs. Since, these simulations are quite time consuming, a limit on the maximum number of iterations of the DE solver has to be placed for practical reasons. Specifically, this bound was set at 350 iterations, which corresponds to about 5700 deterministic crash simulations. Figure 20 shows the convergence of the best candidate point at each iteration for the minimisation of the mean force, for the cases in Section 3.3. For each of these optimisation runs, the best candidate point is not improved for the last 50 iterations before reaching the maximum number of allowed iterations. Hence, this point is accepted as the global minimum with the knowledge that with a large number of additional iterations a better candidate point might be identified. In the authors opinion this is not justified by the additional computational cost that would be required. Note that it is not possible in general to prove that the global minimum is identified using global optimisation approaches in combination with non-convex functions.

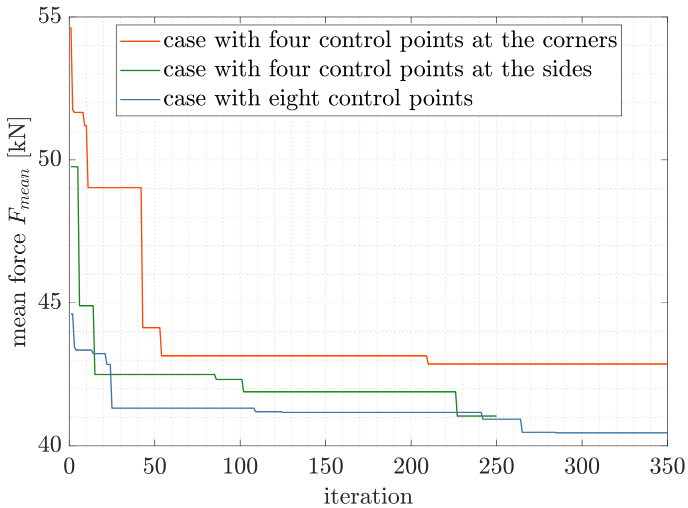

Figure 20: Convergence of the differential evolution algorithm for the minimisation of the mean force, described in section 4.3.2., 4.3.3., and 4.3.4.

In addition, Figure 19 shows that for the multiple independent simulation runs different global minima were identified, which were not always lower than the minima found at a lower interval radius. The bounds of these optimisation runs, marked by a circle, are adjusted to the previously identified minima. One of the reasons for these difficulties is of course the heavy non-linear response of the crash model with respect to the uncertain input parameters. To illustrate this, Figure 21a shows the function evaluation of 5000 samples, for which $X_{1,2}$ are generated by a Latin hypercube and $X_{3,4}$ are set at zero. This figure shows that optimisation of this function is not trivial as there are multiple local minima and maxima, which means that small perturbations of the input parameters can easily lead to a different result. In addition, Figure 21b shows the same data as in Figure 21a represented as a two-dimensional colour plot. The rectangles in Figure 21b represent the input space dimensions that were used in the optimisation runs of Figure 19 with the edge of the figure representing $\Delta x = 65$ MPa. This figure shows the symmetry that exists between the interval field and the rectangular crash box, and some of the local minima and maxima. However, note that because of the interpolation used to create this colour plot some of these local effects are not well-represented. With these challenges in global optimisation of this function in mind it can be argued that the differences between the three cases in Sections 3.3.2, 3.3.3 and 3.3.4 are not that significant. This is especially interesting towards the case with eight control points, in Section 3.3.4 where the dimension of the search space doubled resulting in a much larger computational cost. This case demonstrates that there is a dependence between the number of control points of the interval field and the performance of the component. Hence, it is worthwhile to investigate this dependence as in a more complex case the presence of small triggers, e.g., holes, can lead to bifurcations.

A final point of discussion relates to the use of the peak force and the mean force measure for anti-optimisation of crash structures under uncertainty. Although these measures have a profound physical background and are widely used within the crash community, it is illustrated in Section 3.4 that optimisation on these responses is very hard. In addition, in Section 3.3.4 it is shown that over time the optimisation is more focused on storing energy within the elements than it is at identifying bifurcation modes for the component. Therefore, further investigations should be made to a measure that captures the performance of the overall system with an output that is less prone to small bifurcations in optimisation.

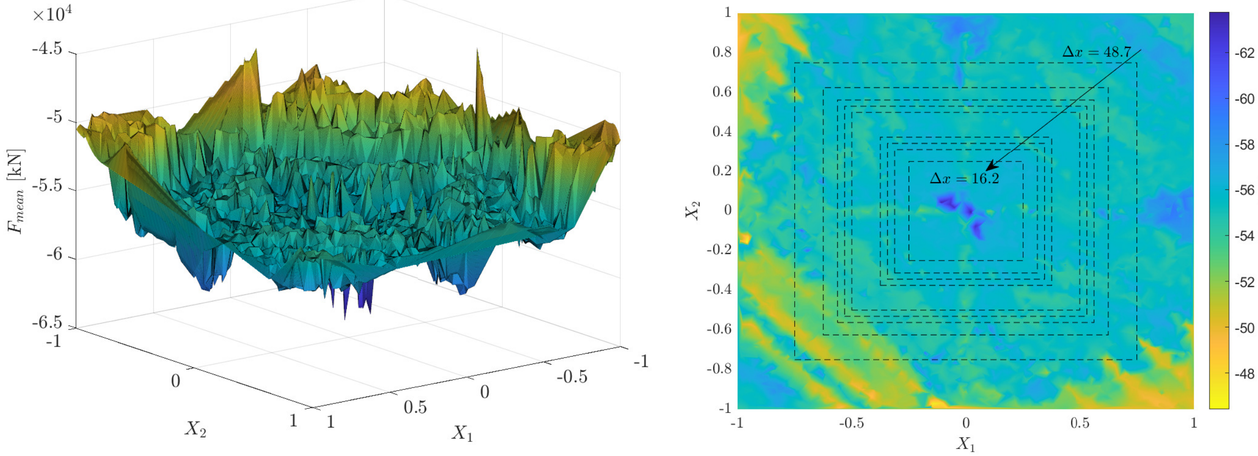

(a) three-dimensional representation of the input and output

(b) two-dimensional representation of the slice

Figure 21: Slice of the input space with the mean force as a response, constructed with 5000 Latin hyper-cube samples for X_1 and X_2 while $X_{3,4} = 0$ the surface is then created by linear interpolation

5. Conclusions

This paper introduces a new framework for modelling and evaluating the crashworthiness of a single component in an early development stage under epistemic uncertainty. This is accomplished by modelling the behaviour of the impacted adjacent structure as unknown but spatially coupled uncertain element stiffnesses. The interval valued performance of the structure is obtained using a global optimisation approach, which is shown to be challenging yet feasible for interval field analysis applied to crash simulation. Based on an academic case study, the results obtained by this innovative framework are demonstrated. The focus is on the sensitivity of the typical main quantities of interest, i.e., mean and peak force during impact, towards the uncertainty included in the interval field modelling strategy. In the presented case study, three dominant deformation modes are identified for the considered range of uncertainty, one of them a global buckling mode. The results indicate that even limited uncertainty in the adjacent structure can affect the deformation mode significantly, resulting in fundamentally different conclusions. In addition, by investigating the realisations of the interval field, the cause of these deformation modes can be further analysed.

Although this work is aimed specifically at crash analysis, this technique can be applied to impact simulations in general. Especially in cases that typically consider fixed boundary conditions while the actual conditions are unknown, the interval field proves to be a powerful concept that allows to tackle uncertainty efficiently. Hence, in future work the combination with the Component Solution Spaces for early stage crash component design is further investigated, which allows for faster design of complex structures in a large and decentralised design process while guaranteeing overall system performance from an early design stage.

Acknowledgements

The authors gratefully acknowledge the support of the Research Foundation Flanders (FWO) under grant 1SA3919N (C. van Mierlo) and 12P3519N (Matthias G.R. Faes). Matthias G.R. Faes further acknowledges the financial support of the Alexander von Humboldt foundation.

References

[1] United nations economic commission for europe (un-ece).
URL https://www.unece.org/trans/main/welcwp29.html

[2] Euro new car assessment programme (euro ncap).
URL https://www.euroncap.com

[3] Global new car assessment programme (global ncap).
URL http://www.globalncap.org

[4] F. Duddeck, Multidisciplinary optimization of car bodies, Structural and Multidisciplinary Optimization 35 (4) (2008) 375–389.

[5] N. Andricevic, F. Duddeck, S. Hiermaier, A novel approach for the assessment of robustness of vehicle structures under crash, International Journal of Crashworthiness 21 (2) (2016) 89–103.

[6] J. Versace, A review of the severity index, Tech. rep., SAE Technical Paper (1971).

[7] O. Boström, M. Y. Svensson, B. Aldman, H.-A. Hansson, Y. Håland, P. Lövsund, T. Seeman, A. Säljö, T. Örtengren, A new neck injury criterion candidate-based on injury findings in the cervical spinal ganglia after experimental neck extension trauma, in: Proceedings of the 1996 International Ircobi Conference on the Biomechanics of Impact, September 11-13, Dublin, Ireland, 1996, pp. 123–136.

[8] Measured data processing vehicle safety workgroup.
URL http://mdvfs.org

[9] M. Daub, Optimizing flexibility for component design in systems engineering under epistemic uncertainty, Phd thesis, Technische Universität München, Munich, Germany (2020).

[10] J. Fender, F. Duddeck, M. Zimmermann, Direct computation of solution spaces, Structural and Multidisciplinary Optimization 55 (5) (2017) 1787–1796.

[11] E. Hilfrich, D. Seidner, Crash safety with high strength steels, presented at international automotive congress, november 1st, Shengyang, China: Verlag Heinrich Vogel.

[12] National highway traffic safety administration (nhtsa), crash simulation vehicle models.
URL https://www.nhtsa.gov/crash-simulation-vehicle-models

[13] S. Hunkeler, F. Duddeck, M. Rayamajhi, H. Zimmer, Shape optimisation for crashworthiness followed by a robustness analysis with respect to shape variables, Structural and Multidisciplinary Optimization 48 (2) (2013) 367–378.

[14] X. Zhao, G. Zhu, C. Zhou, Q. Yu, Crashworthiness analysis and design of composite tapered tubes under multiple load cases, Composite Structures 222 (2019) 110920.

[15] E. İ. Albak, Multi-objective crashworthiness optimization of thin-walled multi-cell tubes with different wall lengths, International Journal of Crashworthiness (2020) 1–18.

[16] G. Sun, H. Zhang, R. Wang, X. Lv, Q. Li, Multiobjective reliability-based optimization for crashworthy structures coupled with metal forming process, Structural and multidisciplinary optimization 56 (6) (2017) 1571–1587.

[17] L. Farkas, D. Moens, S. Donders, D. Vandepitte, Optimisation study of a vehicle bumper subsystem with fuzzy parameters, Mechanical systems and signal processing 32 (2012) 59–68.

[18] A. Khakhali, N. Nariman-Zadeh, A. Darvizeh, A. Masoumi, B. Notghi, Reliability-based robust multi-objective crashworthiness optimisation of s-shaped box beams with parametric uncertainties, International Journal of Crashworthiness 15 (4) (2010) 443–456.

[19] M. Mäck, M. Hanss, Efficient possibilistic uncertainty analysis of a car crash scenario using a multifidelity approach, ASCE-ASME J Risk and Uncert in Engrg Sys Part B Mech Engrg 5 (4).

[20] M. Moustapha, B. Sudret, J.-M. Bourinet, B. Guillaume, Adaptive kriging reliability-based design optimization of an automotive body structure under crashworthiness constraints, International Conference on Applications of Statistics and Probability in Civil Engineering (ICASP) (12th: 2015), 2015.

[21] M. Zimmermann, J. E. von Hoessle, Computing solution spaces for robust design, International Journal for Numerical Methods in Engineering 94 (3) (2013) 290–307.

[22] M. Daub, F. Duddeck, M. Zimmermann, Optimizing component solution spaces for systems design, Structural and Multidisciplinary Optimization 61 (2020) 2097–2109.

[23] M. Daub, F. Duddeck, Maximizing flexibility for complex systems design to compensate lack-of-knowledge uncertainty, ASCE-ASME J Risk and Uncert in Engrg Sys Part B Mech Engrg 5 (4) (2019) 041008.

[24] M. Daub, F. Duddeck, A decoupled design approach for complex systems under lack-of-knowledge uncertainty, International Journal of Approximate Reasoning 119 (2020) 408–420.

[25] M. Faes, D. Moens, Recent trends in the modeling and quantification of non-probabilistic uncertainty, Archives of Computational Methods in Engineering 27 (2019) 633–671.

[26] M. Imholz, M. Faes, D. Vandepitte, D. Moens, Robust uncertainty quantification in structural dynamics under scarse experimental modal data: A Bayesian-interval approach, Journal of Sound and Vibration 467 (2020) 114983. doi:10.1016/j.jsv.2019.114983.

[27] M. Faes, D. Moens, Identification and quantification of spatial interval uncertainty in numerical models, Computers & Structures 192 (2017) 16–33.

[28] E. Vanmarcke, Random fields: analysis and synthesis, World Scientific, 2010.

[29] D. Moens, M. De Munck, W. Desmet, D. Vandepitte, Numerical dynamic analysis of uncertain mechanical structures based on interval fields, in: A. K. Belyaev, R. S. Langley (Eds.), IUTAM Symposium on the Vibration Analysis of Structures with Uncertainties, Springer Netherlands, Dordrecht, 2011, pp. 71–83.

[30] A. Sofi, Structural response variability under spatially dependent uncertainty: Stochastic versus interval model, Probabilistic Engineering Mechanics 42 (2015) 78 – 86.

[31] A. Sofi, G. Muscolino, I. Elishakoff, Static response bounds of Timoshenko beams with spatially varying interval uncertainties, Acta mechanica 226 (2015) 3737–3748. doi:10.1007/s00707-015-1400-9.

[32] A. Sofi, E. Romeo, O. Barrera, A. Cocks, An interval finite element method for the analysis of structures with spatially varying uncertainties, Advances in Engineering Software 128 (2018) 1–19.

[33] M. Imholz, D. Vandepitte, D. Moens, Derivation of an input interval field decomposition based on expert knowledge using locally defined basis functions, in: 1st ECCOMAS Thematic conference on international conference on uncertainty quantification in computational sciences and engineering, 2015, pp. 1–19.

[34] D. Wu, W. Gao, Hybrid uncertain static analysis with random and interval fields, Computer Methods in Applied Mechanics and Engineering 315 (2017) 222–246.

[35] C. Jiang, B. Ni, N. Liu, X. Han, J. Liu, Interval process model and non-random vibration analysis, Journal of Sound and Vibration 373 (2016) 104–131.

[36] B. Ni, C. Jiang, Interval field model and interval finite element analysis, Computer Methods in Applied Mechanics and Engineering 360 (2020) 112713.

[37] M. Faes, D. Moens, On auto- and cross-interdependence in interval field finite element analysis, International Journal for Numerical Methods in Engineering 121 (9) (2020) 2033–2050. doi:10.1002/nme.6297.

[38] D. Moens, M. Hanss, Non-probabilistic finite element analysis for parametric uncertainty treatment in applied mechanics: Recent advances, Finite Elements in Analysis & Design 47 (1) (2011) 4–16.

[39] R. Storn, K. Price, Differential evolution–a simple and efficient heuristic for global optimization over continuous spaces, Journal of global optimization 11 (4) (1997) 341–359.

[40] K. Price, R. M. Storn, J. A. Lampinen, Differential evolution: a practical approach to global optimization, Springer Science & Business Media, 2006.

[41] E. W. Dijkstra, A note on two problems in connexion with graphs, Numerische Mathematik 1 (1) (1959) 269–271.

[42] Livermore Software Technology Corporation (LSTC), Keyword Users Manual Volume 2: Material Models, Vol. II, 2014.

[43] SAE, J211-1.1995 552. doi:10.1520/G0154-12A.

[44] D. Moens, D. Vandepitte, A survey of non-probabilistic uncertainty treatment in finite element analysis, Computer Methods in Applied Mechanics and Engineering 194 (12) (2005) 1527–1555, special Issue on Computational Methods in Stochastic Mechanics and Reliability Analysis.

[45] I. Elishakoff, R. Haftka, J. Fang, Structural design under bounded uncertainty—optimization with anti-optimization, Computers & Structures 53 (6) (1994) 1401–1405.